Identifying the Collapse Hazard of Steel Special Moment-Frame Buildings with Viscous Dampers Using the *FEMA P695* Methodology

H. Kit Miyamoto,[a)] M.EERI, Amir S. J. Gilani,[b)] Akira Wada,[c)] M.EERI, and Christopher Ariyaratana[d)]

An innovative design using steel special moment frames sized per building code requirements for strength and viscous dampers to control story drift ratios results in longer period structures that limit floor accelerations with excellent performance in design-level earthquakes. However, the response of this design to extreme seismic events is not well understood. This is due to the lack of: a) limit state data for dampers, and b) data on the response of the system when subjected to large earthquakes. To address these issues, analytical investigation of the limit states of dampers was performed and the performance of the model was correlated with experimental data. This model was then implemented in a group of archetypes subjected to collapse-level loading. Analysis showed that this design had satisfactory performance when subjected to extreme seismic events. Additional significant improvement in performance was obtained with an enhanced damper design and with a damper safety factor of 1.3. [DOI: 10.1193/1.3651357]

INTRODUCTION

A system consisting of steel special moment-resisting frames and fluid viscous dampers (hereinafter referred to as "SMRF-FVDs") has been used in practice to resist seismic loading. Typically, steel members are sized for the strength level of code-prescribed forces, and the dampers are sized to control drift. Such systems have also been shown to be a cost-effective solution because the expense of the dampers is mitigated by the savings in steel weight (Miyamoto and Gilani 2008) and the design produces better performance in design seismic events (Miyamoto and Singh 2002).

[a)] Tokyo Institute of Technology and Miyamoto International, 700 South Flower Street, Los Angeles, CA 90017
[b)] Miyamoto International, 1450 Halyard Drive, West Sacramento, CA 95691
[c)] Tokyo Institute of Technology, Ookayama, Meguro-ku, Tokyo 152-8550, Japan
[d)] Formerly of the University of Illinois at Urbana-Champaign, 601 East John Street, Champaign, IL 61820

Earthquake Spectra, Volume 27, No. 4, pages 1147–1168, November 2011; © 2011, Earthquake Engineering Research Institute

Although the SMRF-FVD system has been adequate for design-level events, research was conducted to investigate the performance of the system during large events. This research* was based on the *FEMA P695* methodology (NEHRP 2009) and was designed to address the following issues:

- **Damper limit states**. In typical design and analysis, dampers are modeled as a viscous dashpot element in series with an elastic spring. In other words, the limit states of dampers and their effect on the response are not accounted for. For very large earthquakes, it is anticipated that some of the FVDs in the structure will reach their limit states.
- **SMRF-FVD performance in very large earthquakes**. SMRF-FVD systems have not been subjected to large earthquakes. Therefore, it is not known how the system would perform at large or near-collapse shaking levels.
- **FVD factor of safety**. The adequacy of the safety factor used to fabricate the dampers has not been investigated. The current U.S. code provisions for the design of viscous dampers are based on Chapter 19 of ASCE/SEI 7 (ASCE 2005). In this approach, the dampers are constructed with a factor of safety of 1.0 with respect to the computed damper response values at the maximum considered earthquake (MCE) intensity. For retrofit of structures with viscous dampers, a safety factor of 1.3 is recommended by ASCE/SEI 41 (ASCE 2006).

This research addressed these issues by first identifying the limit states of the viscous dampers. Next, analytical studies were conducted to verify the accuracy of the model and to correlate the results with laboratory test data. Finally, incremental dynamic analysis of a group of archetypes of SMRF-FVDs was conducted to assess the performance of the system in very large earthquakes and to assess the adequacy of the code-prescribed factors of safety. The evaluation was based on the *FEMA P695* procedure, which requires that a sufficient number of archetypes be evaluated (using nonlinear analysis) to accurately capture the performance of the system under investigation. In this procedure, the archetypes are selected to represent the variability inherent in a system.

The analysis used a refined viscous damper model that incorporates limit states developed by the authors (Miyamoto et al. 2010b). The analysis and evaluation procedure followed the techniques developed as part of the *FEMA P695* studies. Such an approach has been applied to a variety of building framings (Haselton and Deierlein 2007). One of the objectives of these studies has been to determine the validity of various code parameters, in particular the response modification (R) factor. The material presented in this paper uses a similar methodology. However, the primary objectives of this study were to establish the probability of collapse at MCE and to assess the system performance.

MATHEMATICAL MODEL OF VISCOUS DAMPERS WITH LIMIT STATES

OVERVIEW

Figure 1 (Taylor Devices 2009) presents a cross-sectional view of a typical viscous damper. Viscous dampers consist of a cylinder and a stainless-steel piston. The cylinder is filled with an

* It should be noted that the research was limited in scope. An overall comprehensive investigation of moment-frame structures with viscous dampers is beyond the scope of the work presented in this paper.

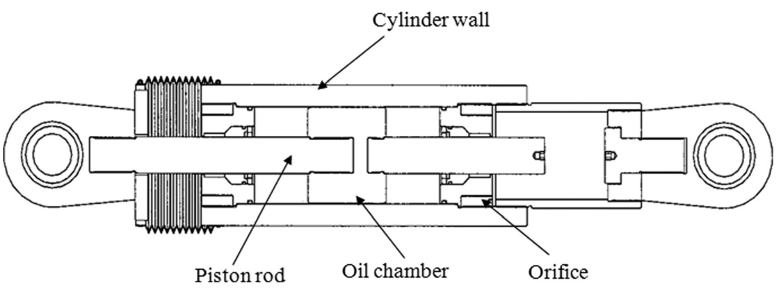

Figure 1. Block diagram for viscous dampers.

incompressible silicone fluid that maintains stable properties over a wide range of operating temperatures. Dampers are activated by the transfer of the silicone fluids between chambers at opposite ends of the unit through small orifices. Typically, the dampers are attached to the structures by hollow structural steel (HSS) members, referred to as "driver braces."

A mathematical representation of FVDs and their driver braces that accounts for the various damper limit states has been developed by the authors (Miyamoto et al. 2010b) and is shown in Figure 2. The viscous damper model consists of the driver brace, piston and piston undercut, the viscous component, and the cylinder walls. Each component has a limit state.

DAMPER LIMIT STATES

The constitutive relations for the various components that were assumed for analysis reported in this paper are presented in Figure 3. The driver brace is used to attach the damper to the beam-to-column connection. The driver is designed using both strength and stiffness criteria. The brace must have sufficient compressive and tensile capacity to withstand the axial load delivered by the damper at the MCE level. Additionally, the driver must be sufficiently stiff to ensure that the viscous element becomes effective. After the brace buckles, the damper is rendered ineffective. It should be noted that the post-buckling

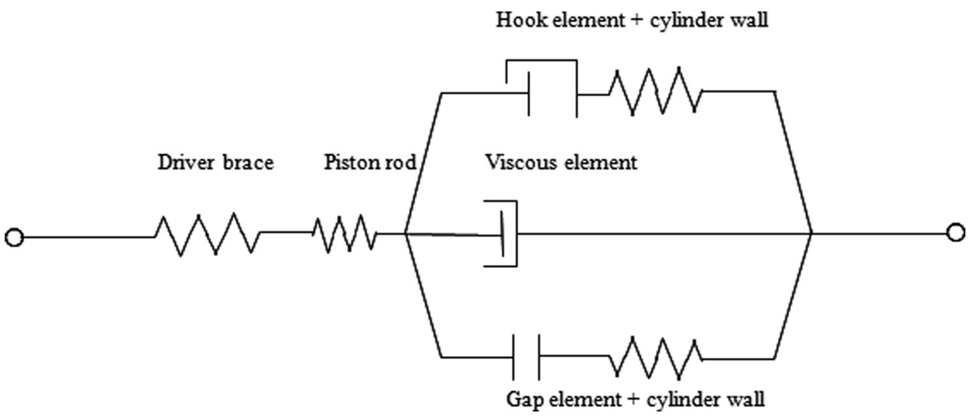

Figure 2. Mathematical representation of the FVD and driver brace.

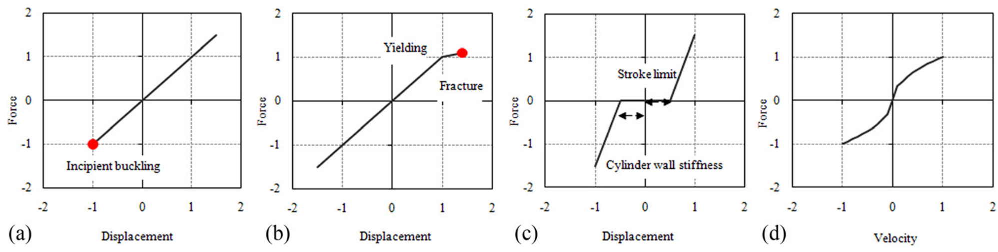

Figure 3. Normalized constitutive relations for viscous damper components: (a) driver brace,[†] (b) piston, (c) cylinder wall, and (d) viscous element.

response of the driver brace has not been modeled for this study because it is assumed that when buckling is initiated, the damper is rendered ineffective given the small tolerance of the piston and the alignment of the unit.

The piston undercut, approximately 13 mm (0.5 in.) long, is the machined-down section of the piston rod between its smooth surface and male threaded part, and it has an area of approximately 80% of the piston rod itself. In compression, the piston undercut yields without buckling because of its short length. In tension, however, its short length causes the undercut section of the piston to yield and then to fracture rapidly after yielding occurs.

If the displacement is less than the available stroke in that direction, the device acts as a viscous damping element. However, when this limit is exceeded, contact between the metal parts at the upper or lower half of the damper will introduce an axial force in the cylinder wall. The elastic stiffness and the capacity of this spring depend on the cylinder properties. The gap (compression only) element has an opening equal to the available stroke, measured from the neutral damper position to the piston's full retracted position. The hook (tension only) element also has an opening equal to the available stroke, but measured from the neutral damper position to the piston's full extended position.

The energy dissipation property of the damper is represented by a viscous element. The force-velocity relation for this element is obtained from:

$$F = Csgn(V)|V|^{\alpha} \tag{1}$$

where C and α designate the damping coefficient and velocity exponent, respectively, and sgn denotes the sign function. The dampers used in this study had a velocity exponent of 0.5—a common value used in U.S. practice. It should be noted that no limit states were considered for the viscous element. For the particular type of dampers investigated in this paper, when the damper velocity exceeds the design velocity multiplied by a damper-specific safety factor, the orifices open further. This, in turn, alters the constitutive properties of the viscous element slightly. More importantly, such a design caps the force delivered to the internal components and protects the cylinder wall from additional pressure loading. A more detailed discussion of

[†] It should be noted that the driver brace is modeled as a linear elastic element. However, the axial force in this component was checked to ensure that the limit state of buckling was accounted for.

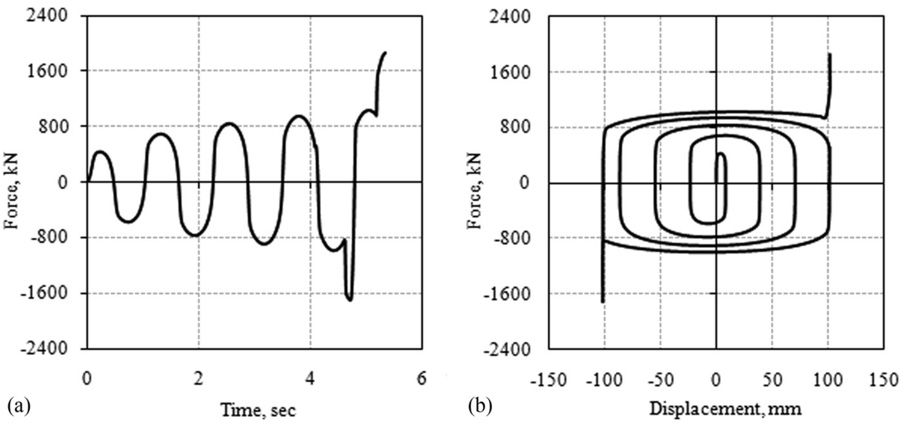

Figure 4. Response of a damper and its components when the piston undercut fractures: (a) force in the element and (b) element force-displacement hysteresis.

this issue is presented in Miyamoto (2010), which shows that ignoring the change in the viscous property of this type of viscous damper does not significantly alter the computed response.

NONLINEAR RESPONSE WITH LIMIT STATES ACTIVATION

Analytical simulations were conducted to investigate the damper response for the activation of the limit states. The damper model in Figure 2 was subjected to sinusoidal loading of increasing amplitude. Data for the case of piston-undercut fracture following the bottoming out of the damper at full piston extension is shown in Figure 4.

At 4.5 s in the response, the piston extension reached the stroke limit and the damper bottomed out. At this point, velocity was zero, and thus the force in the viscous element dropped to zero. The damper acted as an elastic brace. Next, the piston undercut yielded but did not fracture. Loading on the viscous damper was then reversed. This loading reversal resulted in disengagement of the cylinder walls, causing reloading of the viscous component. At 5.3 s, the piston bottomed out again. The damper again became an elastic brace. Loading was increased further, resulting in fracture of the undercut.

The mathematical model of the viscous dampers was prepared to identify the time at which the piston fractured (or the driver brace buckled). At that time, the model underwent spatial transformation, and the damper element was removed from the analysis model using the available commands[†] in the program.

MODEL VERIFICATION

Investigations (Taylor Devices 2009) were conducted to experimentally capture the damper limit states. Next, a mathematical model of a damper with the same properties as the tested unit was prepared. The model incorporated the limit states discussed earlier and

[†] A similar procedure is used in staged-construction analysis, where elements become activated or deactivated (removed).

Table 1. Properties of the laboratory-tested viscous damper

Damping constant	Damping (velocity) exponent	Stroke	Capacity at velocity
195 kN-s/mm (160 kip-s/in.)	0.4	130 mm (5.125 in.)	2,000 kN at 330 mm/s (450 kips at 13 in./s)

was then subjected to the experimental (input) displacement histories. The analytically computed responses (velocity and force) were correlated with the experimental data. It should be noted that for typical applications, more than a single test is required to obtain high confidence in the test data. For the study under consideration, the main reasons for relying on a single test are the following:

- The tests of structural components involve applying force or displacement histories at a low level of loading. Viscous dampers are velocity-dependent devices, and for a failure mode to be activated, large velocities are required. Such high velocities could result in sudden fracture and thus present an inherent safety concern. Furthermore, to reach damper limit states, very large velocities—several times the levels expected at MCE intensity—would be required.
- The test data was used solely to assess the efficacy of the analytical model in capturing various damper limit states. These limit states were captured during the test.

The properties of the laboratory-tested damper are listed in Table 1. This damper was subjected to large-velocity and displacement pulses in succession during laboratory tests. This loading resulted in the damper reaching its limit states. The damper was also subjected to a displacement loading history. To capture its limit states, the piston was extended to within approximately 3 mm (0.125 in.) of its stroke limit in tension prior to being subjected to the test cycles.

The experimental responses are shown as solid lines in Figure 5. The FVD limit states can be identified in this figure:

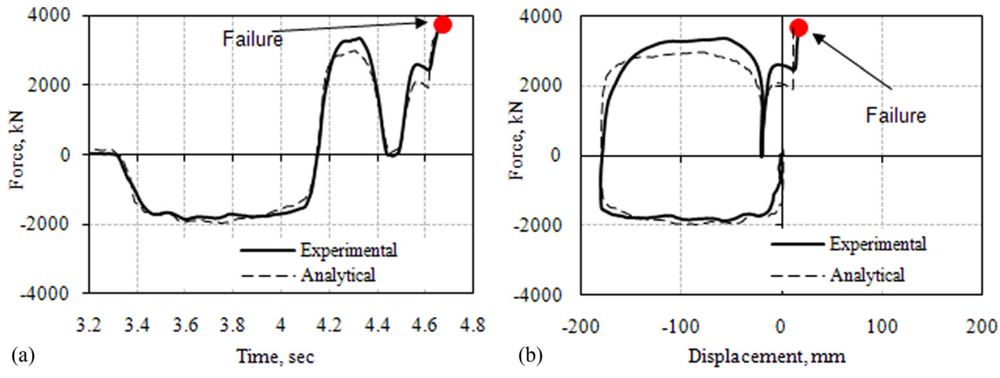

Figure 5. Experimental investigation of damper limit states and analytical correlations: (a) force response and (b) force-displacement hysteresis.

- At 4.3 s, the damper was pulled in tension at 910 mm/s (36 in./s). The displacement input was reversed just before the damper bottomed out. This large velocity was close to 300% of the damper's nominal design value. At this velocity, the internal pressure increased and the cylinder wall expanded, which placed a cap on the rapid rise of the damper force.
- At 4.6 s, the damper bottomed out in tension. As a result, the cylinder walls became activated in resisting the applied displacement, causing a sharp increase in the measured force. This was followed by tensile yielding of the piston undercut. The displacement response after this point was nearly flat (because of yielding in the piston rod), with a slightly increasing slope (because of the stiffness of the cylinder wall).
- At 4.7 s, fracture occurred, and the damper load dropped to zero as the damper became ineffective.

The dashed lines in Figure 5 represent the results obtained from analysis of the damper element. Good correlation was obtained between the experimental data and the analytical simulations. The analytical model captured the damper limit states.

ANALYSIS METHODOLOGY

DESIGN PROCEDURE

Overview

The moment frames used in this study were designed based on the American Society of Civil Engineers' (ASCE) code provisions (ASCE 2005). Member sizes were determined by the strength provisions without regard to lateral-drift limitations. The dampers were then sized to limit the story drift ratios to the maximum code-allowable values.

Seismic Loading

The seismic demand was based on a typical location in the Los Angeles area (importance factor of 1.0, soil type D), with mapped short period (S_s) and 1-second (S_1) spectral accelerations of 1.5 g and 0.6 g, respectively. These values are consistent with the maximum hazard values used in *FEMA P695* (NEHRP 2009). These values place the structures in Seismic Design Category (SDC) D per the ASCE/SEI 7 definition for both the S_s and S_1 spectral intensities.

The design was based on the equivalent-lateral-force (ELF) procedure in ASCE/SEI 7. The redundancy factor (ρ) was equal to 1.0 for all archetypes. ASCE/SEI 7 allows reduction of the design forces by 75% to account for the effect of the redundancy of dampers when supplementary damping is used and when dampers are added to all the floors. However, such a reduction was not taken into account in this study because for some of the archetypes dampers were not added to all the floors. For SMRF structures, the maximum allowable period (T_{max}), as shown in Equation 2, was used in collapse evaluation, as specified by *FEMA P695*. In this equation, C_t and x are period parameters and are equal to 0.028 and 0.8, respectively (with building height, h_n, in ft), T_a is the code-computed estimate of building period, and C_u is the period coefficient and is equal to 1.4.

$$T_{\max} = C_u T_a = C_u C_t h_n{}^x \tag{2}$$

Design of Moment-Frame Members

The provisions of the American Institute of Steel Construction's (AISC) Load and Resistance Factor Design (LRFD) (AISC 2005b) were used to size the members of the SMRFs. Using nominal material properties and appropriate strength reduction factors (ϕ), the beams and columns were designed to resist the code-prescribed load combinations.

The requirements of the AISC seismic provisions (AISC 2005c) for SMRFs were implemented in the design. For example, all members used in the design met the following criteria: strong column-weak beam connections, flange and web compactness of beams and columns, lateral support of beam flanges for lateral torsional buckling, and column slenderness limits. SMRFs with reduced beam sections (RBSs) are one of the prequalified connections (AISC 2005a) for seismic applications. By reducing the beam flange, the plastic hinge is shifted away from the face of the column, and thus the complete joint penetration welds between the beam flange and web-to-column flange are protected. The AISC procedure was used to determine the cut size for the RBS beams. In addition, single column and beam sections per floor were used, and column splices were provided at every third floor, as is typical in design practice.

Design of Dampers

After the moment frames were designed per code requirements for strength, viscous dampers were then sized to limit story drift ratios to the values permitted by the building code. Because dampers have a velocity exponent (α) of 0.5 and because they were not placed on all the floors in a typical model, the linear static and the linear dynamic procedures outlined in the code were not used to size the dampers. Instead, a nonlinear response-history analysis was used.

Three spectrum-matched records were developed, for which the response spectrum closely matched the design spectrum. Figure 6 presents the target spectrum (solid line) and the spectra computed from the three records used in the design (dashed line). The damping constant C, was chosen to limit the story drifts from the maximum responses to the code-prescribed values at the design earthquake intensity. It should be noted that these records were used to determine the damper size only and were not used in further analysis.

Next, the archetypes were subjected to the same three records at the MCE intensity, and the maxima of responses (damper force and displacement) were extracted. This data was then modified using the applicable safety factor for each particular archetype. The modified data was supplied to the damper manufacturer (Taylor Devices 2009), which used these values to design and size the components of the viscous damper.

INPUT HISTORIES FOR COLLAPSE ANALYSIS

The input histories used in analysis were based on the two components of the 22 far-field Next Generation Attenuation (NGA) records (PEER 2009a). These 44 records have been identified by *FEMA P695* for collapse evaluation analysis. The Pacific Earthquake Engineering Research (PEER) Center's NGA database consists of more than 3,500 records for more than 160 events. The 22 records selected correspond to a relatively large sample of

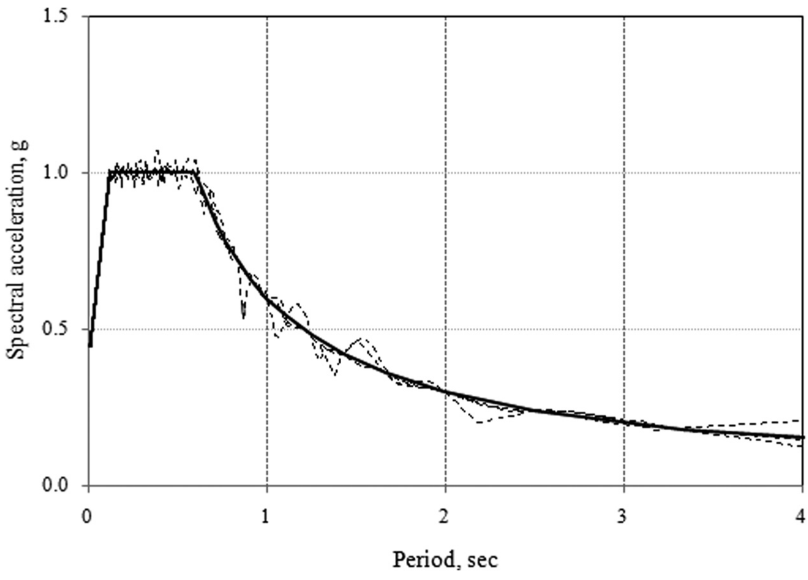

Figure 6. Design-level spectrum (solid line) and response spectra from three pairs of spectrum-matched records used to size dampers.

strong recorded motions that are consistent with the code and are structure-type and site-hazard independent.

Figure 7 presents the acceleration response spectra for these records. These records were used for the collapse analysis of the archetypes discussed in this paper. The MCE spectrum is shown as a solid line in the figure. For analysis, the 44 records were first normalized and then scaled. The records were normalized to remove the record-to-record variation in intensity. The normalization factors used in this study are identical to the values used by *FEMA P695* (NEHRP 2009). The normalized records were then incrementally scaled until one of the criterion for incipient collapse, discussed later in this paper, was reached.

ANALYSIS PROCEDURE

The program OpenSees (PEER 2009b) was used to conduct nonlinear analysis. Models were two-dimensional and used linear beam and nonlinear beam-column elements for SMRF member representation, concentrated plastic hinges to represent RBSs, and a model of Figure 2 for viscous dampers. For the SMRF columns, the procedure described in ASCE/SEI 41 (ASCE 2006) was used to determine the multilinear moment-rotation relations. The elastic concentrated rotational spring constant for the RBS hinges was obtained by fitting the archetype properties to the available experimental data. The moment-rotation behavior for the RBS rotational spring of the SMRF was derived from the deterioration modeling parameters developed by Lignos and Krawinkler (2007), which uses parallel bilinear material definitions. The various components of the viscous damper identified in Figure 2 were modeled as follows:

- The driver brace was modeled using the program's beam-column element. This element was modeled as elastic, and the flag was placed to identify incipient buckling.

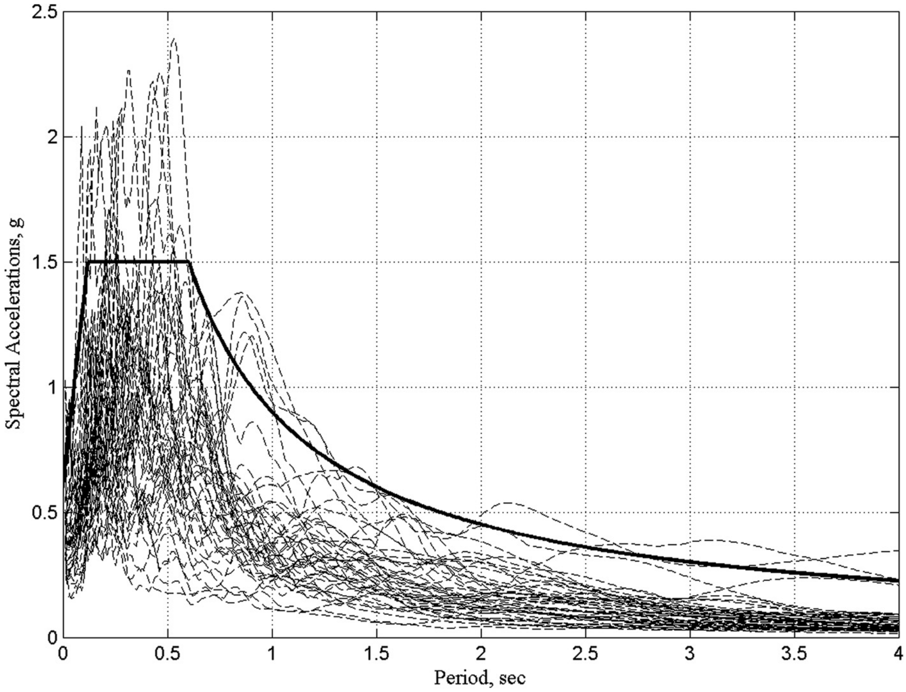

Figure 7. Response spectra for the original (unscaled) 44 PEER NGA far-field records used in collapse analysis (MCE spectrum shown as solid line).

The properties of this element were based on its nominal section properties.

- The piston rod was modeled using a bilinear beam-column element. The elastic stiffness, yield, and ultimate capacity for this element were obtained from the manufacturer.
- The cylinder wall was modeled using a combination of gap and hook elements and elastic beam-column elements to account for the available stroke limit and the stiffness of the cylinder wall, respectively.
- The damper's viscous element properties (velocity coefficient, velocity exponent, force capacity, and stroke) were based on the nominal values obtained from the design of dampers at the MCE intensity.

The models were preloaded with concentrated gravity loads prior to seismic analysis. Lumped-mass representation was used for the model. Inherent damping was assumed as mass- and stiffness-proportional and equaled 2% of critical for modes one and three.

ANALYSIS PROGRAM AND EVALUATION PROCEDURE

OVERVIEW

The following sections present a brief overview of the methodology used by *FEMA P695* to compute the seismic response of archetypes at collapse-level intensity. This discussion has been modified to represent the archetypes and procedures that were used specifically for the data reported in this paper.

PUSHOVER ANALYSIS

Nonlinear static (pushover) analysis of the models is conducted to compute the system ductility, which is used to compute the spectral shape factor (*SSF*) for collapse probability calculations. The *SSF* modification is used to correct the spectral shape of the records for very large earthquakes because the frequency content differs from that of earthquakes with lesser intensities in these events.

The pushover load pattern is selected to simulate the displaced shape from a response spectrum analysis. The target displacement is selected as the horizontal drift at the roof. For structures with dampers, the pushover model includes the damper. Because viscous dampers are velocity-dependent components, they are not activated in static analysis as long as the limit states are not reached. However, after the damper bottoms out, it becomes a stiff diagonal member. Such a member will affect the pushover response significantly.

The pushover analysis results in a nonlinear force-displacement output. A bilinear curve is then fitted to the nonlinear pushover curve and used to compute the yield (δy) and ultimate (δu) roof displacement drifts. The pushover curve on the tensile side is used in computations of ductility ratios (μ_T). The computation of the *SSF* is based on the following equations from *FEMA P695*:

$$\mu_T = min\left(\frac{\delta u}{\delta y}, 8.0\right) \quad (3)$$

$$SSF = e^{0.14(\mu_T - 1)^{0.42}(1.5 - 0.6(1.5 - T_{max}))} \quad (4)$$

INCREMENTAL DYNAMIC ANALYSIS

Incremental dynamic analysis (IDA) simulation (Vamvatsikos and Cornell 2005) is a powerful tool that is used to determine the collapse response of structures. Of interest for this study was the computed IDA plot of the maximum floor drift versus input spectral intensity.

For collapse analysis, the normalized records are scaled and applied to the models to obtain sufficient data points to determine the nonlinear response up to collapse. In this paper, collapse is defined as the lesser of the following drift ratios:

- 18%. This is an arbitrary value that has been used by other researchers (Haselton and Deierlein 2007) when performing similar types of analysis. It should be noted that for models analyzed in this paper, collapse occurred at much smaller values. Furthermore, given the limitations in the models described here (for example, using lumped plasticity), phenomena such as beam flange and web local buckling were not captured, and these would occur at drifts of less than 18%. However, the 18% value was used as a benchmark when an analysis case did not converge numerically.
- At a point on the descending slope of the force-deformation curves when the tangent stiffness is reduced to 5% of the initial elastic stiffness.

After the IDA has been completed for a structure, the collapse spectral intensities (S_a) for the 44 records are tabulated and the median of the collapse data is used for further analysis. This value is labeled as the median collapse capacity (S_{CT}). The MCE spectral acceleration at T_{max} is designated as S_{MT}. The collapse margin ratio (CMR) is then computed from the following:

$$CMR = \frac{S_{CT}}{S_{MT}} \tag{5}$$

The adjusted collapse margin ratio ($ACMR$) is then computed, as shown in Equation 6, to adjust the computed CMR for the spectral shape:

$$ACMR = SSF * CMR \tag{6}$$

COLLAPSE FRAGILITY CURVE (PROBABILITY OF COLLAPSE AT MCE)

The 44 collapse points obtained from the IDA of a response quantity are statistically organized. The collapse data is treated as a random variable whose logarithm is normally distributed. A lognormal cumulative distribution function (CDF) is fitted to the data to obtain the theoretical mean (and median) and standard deviation of the data. Although useful, such a distribution does not account for all the uncertainties present in analysis and does not include the *SSF*. As such, the following two modifications are required:

1. *FEMA P695* provides recommendations for the total system collapse uncertainty (β_{tot}). For the analysis presented in this paper, superior (A) quality of both the test data and the model was assumed.[&] This assumption yielded a β_{tot} of 0.55. The CDF was then plotted with the computed mean, but with a standard deviation of 0.55 for the logarithm of the random variable (S_a).
2. For the structural system, the CDF was then modified to account for the difference between the *ACMR* and the *CMR* as represented by the *SSF*. The ordinate of this plot at the MCE intensity presents the probability of collapse at that intensity.

For structures with viscous dampers, the intensity when the damper bottoms out (stroke limit) or fails (force limit) is of particular interest. Fragility plots of these quantities for the dampers provide important information on the adequacy of the damper properties and the effect of the damper factor of safety on the response. These fragility plots are also presented with a total uncertainty of 0.55 without the *SSF* modification. Such an approach is conservative because it will overestimate the number of viscous dampers reaching a limit state.

[&] It should be noted that a single test of a damper would not typically merit a superior rating. As such, a high rating is reserved for when significantly more test data points are available. In this paper, selection of the superior rating was based on the following: a) use as an illustration—intended to provide consistency with similar work by other researchers; b) demonstration of superior quality control—the high degree of precision involved in manufacturing viscous dampers, compared with more typical structural elements; and c) limited use of test data—the experimental data are used solely to calibrate the proposed modeling approach. In other words, the damper and SMRF properties and performance used in the archetypes are independent of the test data presented in this paper.

ARCHETYPES

The seismic performance of the steel SMRF-FVD structural system was investigated by considering the behavior of ten archetypes. The archetypes are intended to serve as prototypes of the building configuration for which the system is ideally suited. For the purposes of this investigation, the SMRF-FVD archetypes comprised one-, two-, and five-story structures. These low- to mid-rise buildings are an important subgroup of structures, because many applications of the SMRF-FVD system are for this type of construction. A companion paper addresses the response of high-rise SMRF-FVD buildings (Miyamoto et al. 2010a).

The archetypes were developed to investigate both the boundary condition of the first-floor columns and the design methodology used to size the dampers. For the code-compliant archetypes, the following assumptions were made: a) a damper constant was selected to limit the drift ratios to the code-prescribed values (2% or 2.5%, depending on the number of stories), and b) a factor of safety of 1.0 was used to size the damper components. For a second subset of the archetype group, the following assumptions were made: a) a damper constant was selected to limit the drift ratios to 1%, and b) a factor of safety of 1.3 was used to size the damper components. The latter design criterion is often used for above-code seismic performance (Miyamoto and Gilani 2008) and is hereinafter referred to as "enhanced design."

ANALYSIS MATRIX

For each story configuration, pertinent damper configurations and column support conditions were evaluated. Following usual practice standards, the dampers were

Table 2. List of archetypes used in analysis

Archetype	Configuration			Design			Dampers	
				Period, s				
ID	Stories	Column base	Mass, Mg	T_n	T_{max}	Drift	FS	Floors
1PC	1	Pinned	116	1.13	0.31	2.5%	1.0	1
1PE	1	Pinned	116	1.13	0.31	1.0%	1.3	1
1FC	1	Fixed	116	0.42	0.31	2.5%	1.0	1
1FE	1	Fixed	116	0.42	0.31	1.0%	1.3	1
2PC	2	Pinned	808	1.55	0.53	2.5%	1.0	1
2PE	2	Pinned	808	1.55	0.53	1.0%	1.3	1
2FC	2	Fixed	808	1.14	0.53	2.5%	1.0	1
2FE	2	Fixed	808	1.14	0.53	1.0%	1.3	1
5FC	5	Fixed	2172	2.13	1.11	2.0%	1.0	1, 2, 3
5FE	5	Fixed	2172	2.13	1.11	1.0%	1.3	1, 2, 3, 4

T_n denotes the fundamental period obtained from modal (eigenvalue) analysis.
FS is the factor of safety.
Archetype designations: xyz, where x designates number of stories (1, 2, 5), y designates column boundary condition (pinned or fixed), and z denotes factor of safety (code or enhanced).

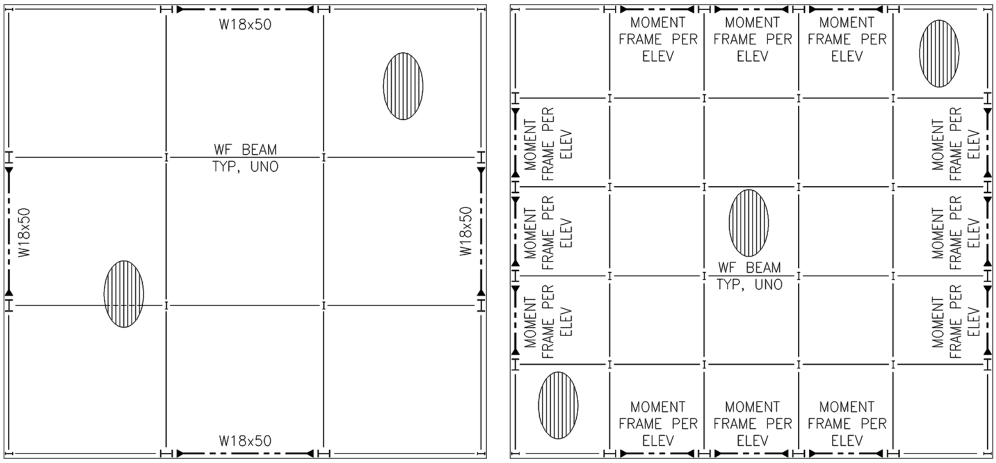

Figure 8. Archetype plan views: (a) one-story models and (b) two- and five-story models.

typically concentrated at the lower floors. Table 2 presents the archetype matrix used in analysis.

ARCHETYPE GEOMETRY

For all archetypes, first floor and typical story heights were 4 m, and typical bays were 9.1 m wide. The plan view for the one-story archetypes is presented in Figure 8a. The one-story frame was square in plan, measured 27 m (90 ft) on each side, had three bays, and had a single-bay perimeter SMRF on each side. For the two- and five-story archetypes, the floor plan in each direction consisted of five equal bays. The SMRFs were provided only along the perimeter (as is typical industry practice in the United States) and along three consecutive interior bays. The archetypes were symmetrical, and floor diaphragms were modeled as rigid. Two-dimensional modeling along one of the principal directions was used to characterize the response of the structures.

Figure 9 presents the elevation view of the archetypes used in analysis. For the single-story archetypes, the column size was governed by the slenderness limit, and both fixed and pinned column cases had identical members. For the two- and five-story models, each model represented an exterior framing in the east–west direction. The models accounted for the three-bay SMRFs and the two exterior gravity-frame bays. One more gravity bay was placed on each side of the archetypes to account for the combined stiffness of all interior gravity columns. Such an inclusion is a deviation from the methodology used by *FEMA P695*. However, these supercolumns were included in the model to realistically assess the collapse performance of the building after the dampers and the SMRFs had reached their limit states. Each supercolumn had a stiffness that was four times the nominal interior column stiffness. For these columns, the flexural capacity was computed as the sum of the moment capacity of the interior columns. Fiber-element plastic hinges were used to capture the yielding of these components.

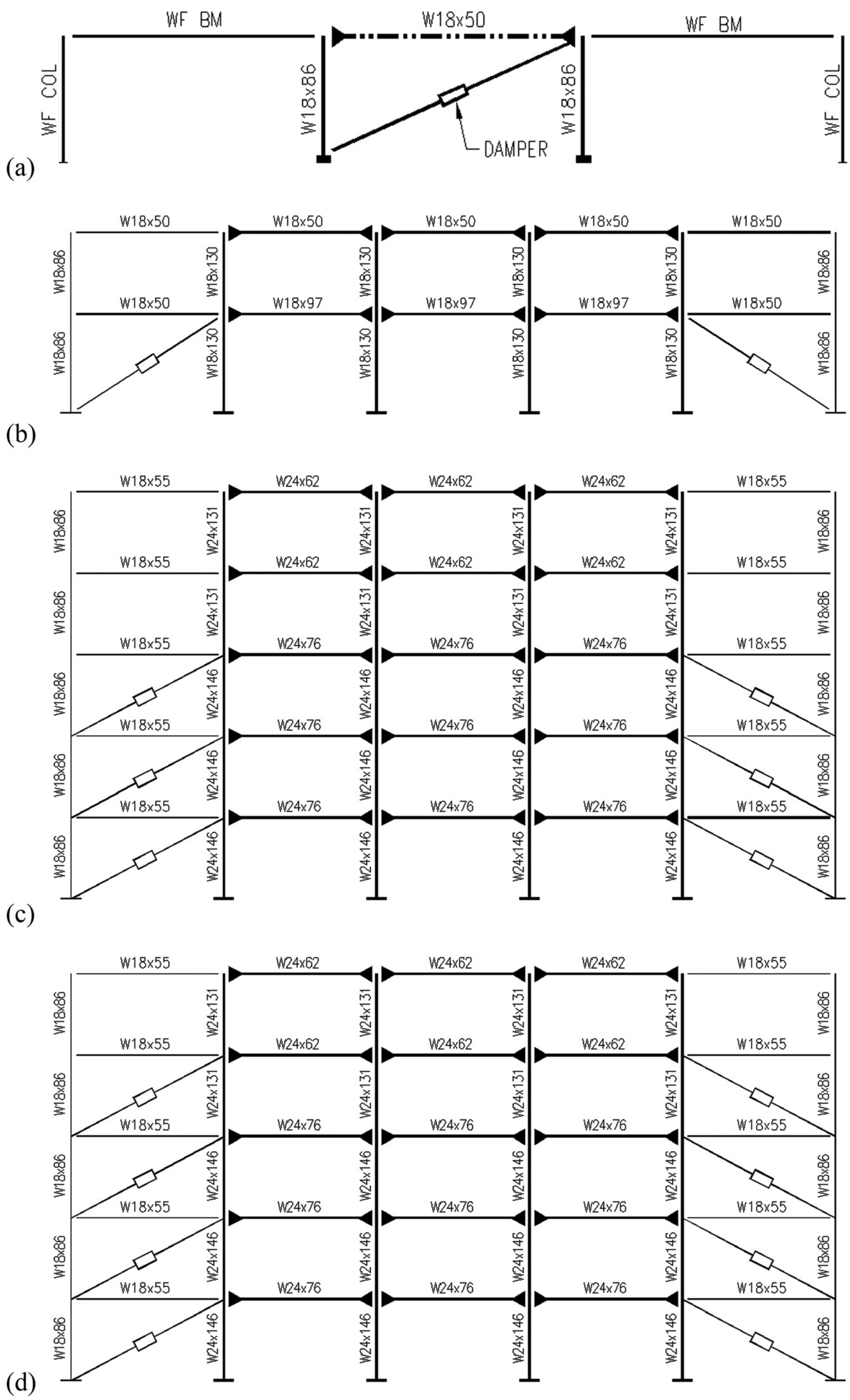

Figure 9. Elevation views of archetypes: (a) one-story, (b) two-story, (c) five-story fixed-base 2% drift, and (d) five-story fixed-base 1% drift.

ANALYSIS RESULTS

PUSHOVER ANALYSIS RESULTS

Figure 10 presents the pushover curves for archetypes 5FC and 5FE. Because the dampers were placed symmetrically for multistory archetypes, the pushover curves were symmetrical. Therefore, results for only one quadrant are shown. For the one-story archetypes, only a single damper was used, and as such the pushover curve depended on whether the driver brace and piston rod were loaded in tension or compression.

The dashed lines in Figure 10 correspond to the bare fame (no dampers included in the analysis), and the solid lines show the plot for the archetypes. The effect of including dampers in analysis is shown by the difference in the two plots. Note that because viscous dampers are velocity-dependent devices, they do not influence the pushover response until the damper bottoms out. A typical pushover curve consists of the following: a) an elastic portion, b) yielding in the SMRF members, c) significant increase in capacity and stiffness as dampers bottom out, and d) sudden reduction in strength as dampers experience a loss of capacity because of tensile fracture of the piston undercut or buckling of the driver brace. This pattern is followed by the SMRF members reaching their capacity strength and the structure unloading.

For archetypes with several dampers, the descending slope of the damper failure comprises several segments, each corresponding to failure along a floor. For cases with a 1.0 factor of safety, the tensile capacity of the piston undercut is significantly smaller than is the compression capacity of the driver brace. For these cases, the tensile failure precedes the compressive failure and results in two distinct drops in the curves (see Figure 10a). For cases with a factor of safety of 1.3, the tensile and compressive capacities of the dampers are more closely spaced, therefore the sharp drops in the system stiffness are closer in the plot (see Figure 10b).

Systems with large factors of safety have higher capacities but smaller deformation ductility. This difference is primarily because when a larger factor of safety and a smaller allowable drift ratio were used for the enhanced design, the dampers had a smaller design stroke. The computations for the *SSF* are presented in Table 3. For all cases, the *SSF* value is between approximately 1.2 and 1.5. The *SSF* serves to increase the collapse capacity (NEHRP 2009).

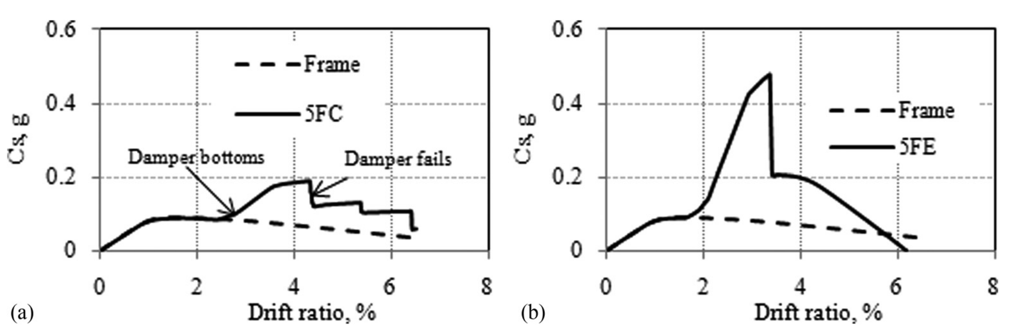

Figure 10. Pushover curves for the models: (a) archetype 5FC and (b) archetype 5FE.

Table 3. Archetype pushover analysis results

Archetype	1PC	1PE	1FC	1FE	2PC	2PE	2FC	2FE	5FC	5FE
δ_y	0.016	0.016	0.010	0.010	0.016	0.016	0.012	0.012	0.010	0.013
δ_u	0.188	0.246	0.675	0.550	0.100	0.045	0.090	0.047	0.064	0.052
μ_T	8.0	8.0	8.0	8.0	6.3	2.8	7.7	4.0	6.3	4.0
SSF	1.34	1.34	1.34	1.34	1.31	1.21	1.34	1.25	1.45	1.36

δ_y and δ_u denote the yield and ultimate displacement (drifts), respectively.
μ_T is the system ductility.
SSF is the spectral shape factor.

IDA RESULTS

Figure 11 presents the IDA plots for the archetypes 5FC and 5FE. It should be noted that for a majority of the analyses, the IDA plots flatline (indicating collapse) at approximately 6% to 7% drift ratio. The thick solid and the thick dashed horizontal lines in Figure 11 denote the S_{MT} and S_{CT} spectral intensities, respectively. The calculations for the *ACMR* are presented in Table 4.

The *ACMR*s for the archetypes vary from 2.1 to 5.4. As such, all the archetypes meet *FEMA P695* requirements, which set an acceptable collapse margin ratio at 1.6 for an individual archetype. These results show that the SMRF-FVD system is dependable, with a relatively large margin against collapse at the MCE intensity. It should be further noted that adding a relatively small (1.3) factor of safety to the damper stroke and force capacities increases the *ACMR*s significantly, from 2.7 to 3.5, or an increase of 30%.

COLLAPSE MECHANISM

Several collapse mechanisms were identified for the archetypes. In each case, the collapse was initiated by the instability of an individual floor or by the instability of two adjacent floors, as listed in Table 5 for the five-story archetypes. For archetype 5FC, a large

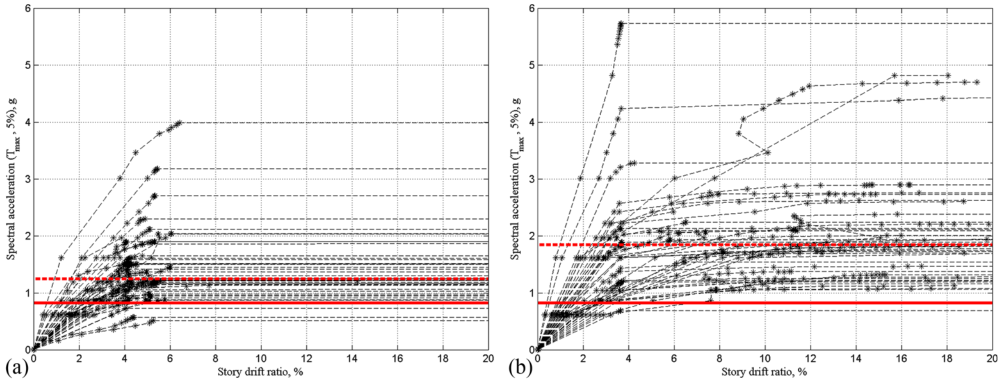

Figure 11. IDA plots for the models: (a) archetype 5FC and (b) archetype 5FE.

Table 4. Archetype IDA results

Archetype	1PC	1PE	1FC	1FE	2PC	2PE	2FC	2FE	5FC	5FE
S_{CT} (g)	2.79	3.49	5.27	6.12	2.38	3.77	2.59	3.39	1.24	1.84
S_{MT} (g)	1.50	1.50	1.50	1.50	1.50	1.50	1.50	1.50	0.82	0.82
CMR	1.86	2.32	3.51	4.08	1.59	2.51	1.72	2.26	1.51	2.25
ACMR	2.4	3.1	4.7	5.4	2.1	3.0	2.3	2.8	2.2	3.1

S_{CT} is the median spectral acceleration at collapse.
S_{MT} is the MCE spectral acceleration.
CMR is the collapse margin ratio.
ACMR is the collapse margin ratio adjusted for the spectral shape.

number of collapses resulted from instability in the floors above the level at which the dampers were terminated. For archetype 5FE, almost all the collapse cases corresponded to instability at the first floor. Although the first-floor damper had a factor of safety of 1.3, it was designed for a drift ratio of 1.0% and thus had a small stroke capacity. Therefore, the damper at the first floor bottomed out and then failed, causing a soft-story mechanism for this archetype. Such a failure mode can be mitigated by specifying larger damper factors of safety for the stroke at the bottom story of structures.

COLLAPSE FRAGILITY ANALYSIS

Figure 12 presents the collapse fragility plots for archetypes 5FC and 5FE. In this figure, the analytically computed data points are represented by asterisks. As noted earlier, the test data and curve were fitted and then adjusted to account for system uncertainty and the *SSF* effect. This final curve is represented by the solid lines. The medians and probabilities of failure at the MCE intensity are marked with dashed lines in the figures and are listed in Table 6. For all the archetypes, this probability ranged from 0.1% to 9%.

FEMA P695 provides two limiting values of acceptable probability of collapse at the MCE intensity for a structural system: a) 20% for individual archetypes, and b) 10% for the computed average of the entire archetype group. Both of these limits must be satisfied for acceptable performance. It should be noted that the values listed in Table 6 imply an acceptable performance for the structural systems investigated in this paper.

As shown in Figure 12 and Table 6, adding the 1.3 factor of safety to the damper components resulted in a two- to fourfold reduction in collapse probability. Such an increase in damper size is cost-effective, and it would significantly improve the response of the damped SMRF-FVD structures when they are subjected to large earthquakes.

Table 5. Archetype collapse analysis

Archetype	Two levels	5th	4th	3rd	2nd	1st	Sum
5FC	18%	54%	–	16%	7%	5%	100%
5FE	0%	–	2%	–	–	98%	100%

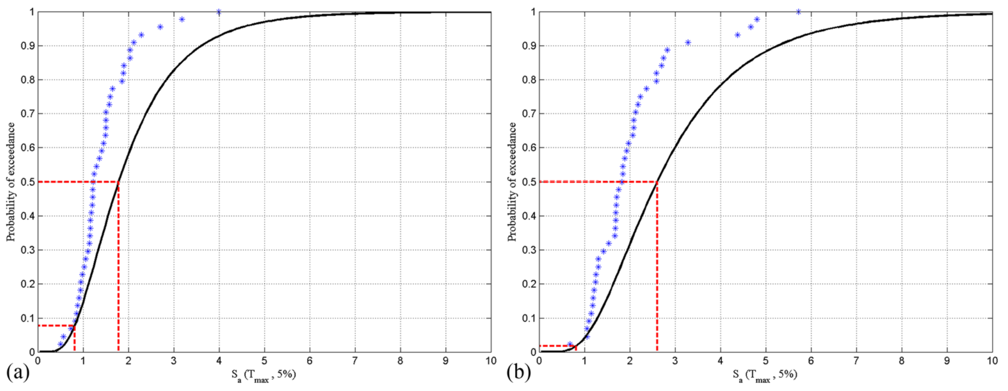

Figure 12. System fragility plots for the models: (a) archetype 5FC and (b) archetype 5FE.

DAMPER RESPONSES

Figure 13 presents the damper fragility plots for the stroke and force, respectively, for archetype 5FC. In this figure, the analytically computed data points are represented by asterisks. As noted earlier, the test data and curve were fitted and then adjusted to account for system uncertainty. The final curve is represented by the solid lines. The medians and probabilities of failure at the MCE intensity are marked with dashed lines in the figures.

The probability of reaching the damper stroke and force limit states is approximately 33% and 24%, respectively. Table 7 lists the median intensity for the dampers reaching the limit states and the probability of reaching limit states at the MCE intensity. The average probabilities of reaching the stroke and force limit states at the MCE intensity for the code-minimum design were 26% and 16%, respectively. It was noted that when a factor of safety larger than the code minimum was included in the damper design, the average probability of reaching the stroke or the force limit state at the MCE intensity was reduced to 9% and 6%, respectively (or a reduction by a factor of approximately 2.8). It is therefore important to use a high safety factor and quality dampers for reliable performance.

SYSTEM PERFORMANCE

Table 8 summarizes the performance of the ten archetype indexes and the system of the archetypes. For acceptable performance, *FEMA P695* specifies a minimum *ACMR* value of 2.0 for a group of archetypes and a minimum *ACMR* of 1.6 for the worst archetype

Table 6. Archetype collapse fragility analysis

Archetype	1PC	1PE	1FC	1FE	2PC	2PE	2FC	2FE	5FC	5FE
Pr_{ColMCE} (%)	5	2	0.3	0.1	9	2	6	3	8	2

Pr_{ColMCE} (%) is the probability of collapse at the MCE level with a total system uncertainty ($\beta_{To\tau}$) of 0.55.

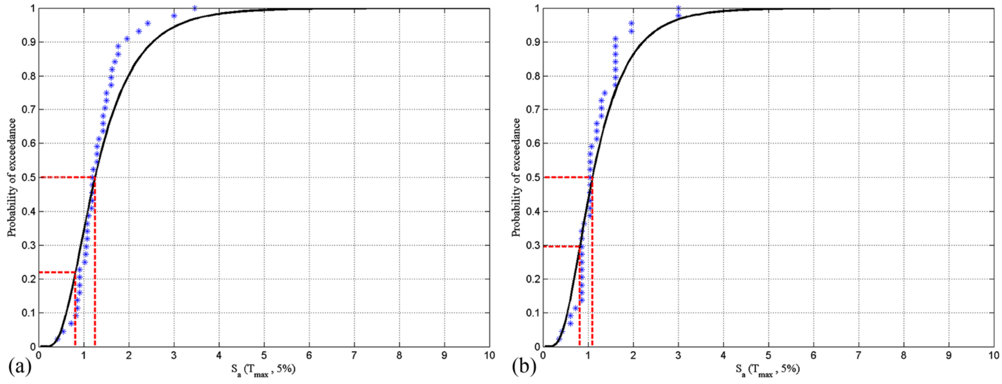

Figure 13. First-story damper fragility plots for archetype 5FC: (a) stroke and (b) force.

Table 7. Damper fragility analysis

Archetype		1PC	1PE	1FC	1FE	2PC	2PE	2FC	2FE	5FC	5FE	C_{avg}	E_{avg}
S_a* (g)	Stroke	2.6	2.8	3.3	3.3	1.6	3.4	2.0	3.1	1.1	1.6	–	–
	Force	3.0	3.8	4.8	4.8	2.3	3.9	2.2	3.4	1.2	1.6	–	–
*Pr** (%)	Stroke	15	12	8	8	45	7	31	9	33	11	26	9
	Force	10	5	2	2	21	4	24	7	22	10	16	6

S_a* is the median spectral intensity for the damper limit states.
Pr* denotes the probability of reaching the damper limit states at the given MCE intensity.
C_{avg} is the average of the code-minimum design (factor of safety = 1.0); archetypes 1PC, 1FC, 2PC, 2FC, and 5FC.
E_{avg} is the average of the enhanced design (factor of safety = 1.3); archetypes 1PE, 1FE, 2PE, 2FE, and 5FE.

Table 8. System performance

Archetype	1PC	1PE	1FC	1FE	2PC	2PE	2FC	2FE	5FC	5FE	S_{avg}	C_{avg}	E_{avg}
Stories	1	1	1	1	2	2	2	2	5	5	–	–	–
ACMR	2.4	3.1	4.7	5.4	2.1	3.0	2.3	2.8	2.2	3.1	3.1	2.7	3.5
Pr_{ColMCE} (%)	5	2	0.3	0.1	9	2	6	3	8	2	–	6	2
*ACMR*_Accept	1.6	1.6	1.6	1.6	1.6	1.6	1.6	1.6	1.6	1.6	2.0	2.0	2.0
$Pr_{ColMCE_}$Accept (%)	20	20	20	20	20	20	20	20	20	20	10	10	10
Check	P	P	P	P	P	P	P	P	P	P	P	P	P

S_{avg} is the average of the ten archetypes.
C_{avg} is the average of the code-minimum design (factor of safety = 1.0); archetypes 1PC, 1FC, 2PC, 2FC, and 5FC.
E_{avg} is the average of the enhanced design (factor of safety = 1.3); archetypes 1PE, 1FE, 2PE, 2FE, and 5FE.
P indicates pass, and F indicates fail.

performance within the group. The acceptable probability of collapse at MCE intensity is 10% on average and 20% for the worst-case archetype in a group. It should be noted that all the archetypes individually and the system as a group meet these requirements. Therefore, they individually, and as a system, are labeled as "Pass," given their acceptable performance. The archetypes have at least a margin of safety of 2.0 compared with acceptable thresholds. Thus, it can be expected that the low- and mid-rise SMRF-FVDs using the code-recommended factor of safety (1.0) will perform adequately in large earthquakes. The collapse probability at the MCE level is reduced by a factor of approximately 3 when a nominal (1.3) factor of safety is included in the design of the damper components.

SUMMARY AND CONCLUSIONS

IDA of SMRF-FVD archetypes was carried out to assess the probabilistic response of this design in large earthquakes. A detailed model of the FVDs, incorporating the damper limit states, was included in the archetypes evaluated. The archetypes were then subjected to pushover analysis and IDA, and the collapse margin and the collapse probability at the MCE intensity were determined. Based on the analytical results, the following conclusions were made:

- The mathematical model of dampers incorporating the damper limit states can be used to represent the physical properties of viscous dampers and the effect of these properties on structural response. This model correlates well with experimental data.
- The SMRF-FVD system, using the code minimum factor of safety, provides adequate performance at the MCE and large earthquake intensities. The system has sufficient margin against collapse and a probability of collapse at the MCE intensity that is below the FEMA-recommended values.
- The SMRF-FVD system that uses both an enhanced design and a damper factor of safety of 1.3 has a larger margin against collapse than does the code-minimum SMRF-FVD system. The probability of collapse at the MCE level is reduced by an average factor of 3.0, and the protection provided to the dampers in large earthquakes is increased by an average factor of 2.8.
- For the one- and two-story archetypes, when the bases of the columns were fixed, the performance was improved. This improvement was more pronounced for the single-story archetypes. Further study is needed to determine whether this finding can be extended to taller structures.
- For the five-story archetypes, the enhanced performance objective of 1% drift resulted in an almost exclusive first-level soft-story mechanism. Further investigations are currently underway to determine the effect on the collapse shape of five-story archetypes when using a larger stroke factor of safety for the bottom-story dampers.

ACKNOWLEDGMENTS

The authors wish to acknowledge financial support from Taylor Devices and Armour Steel. The technical assistance of Mr. Doug Taylor and Mr. John Metzger of Taylor Devices is also acknowledged.

REFERENCES

American Institute of Steel Construction (AISC), 2005a. *Prequalified Connections for Special and Intermediate Steel Moment Frames for Seismic Applications, ANSI/AISC 358-05*, Chicago, IL.

American Institute of Steel Construction (AISC), 2005b. *Seismic Provisions for Structural Steel Buildings, AISC 341-05,* Chicago, IL.

American Institute of Steel Construction (AISC), 2005c. *Specification for Structural Steel Buildings, AISC 360-05*, Chicago, IL.

American Society of Civil Engineers (ASCE), 2005. *Minimum Design Loads for Buildings and Other Structures, ASCE/SEI 7-05*, Reston, VA.

American Society of Civil Engineers (ASCE), 2006. *Seismic Rehabilitation of Existing Buildings, ASCE/SEI 41-06*, Reston, VA.

Haselton, C. B., and Deierlein, G.G., 2007. *Assessing Seismic Collapse Safety of Modern Reinforced Concrete Moment Frame Buildings*, *Report No. TR-156*, John A. Blume Earthquake Engineering Center, Stanford University, Palo Alto, CA.

Lignos, D. G., and Krawinkler, H., 2007. A database in support of modeling of component deterioration for collapse prediction of steel frame structures, *Proceedings of ASCE Structures Congress*, Structural Engineering Institute, Long Beach, CA.

Miyamoto, H. K., 2010. *Probabilistic Seismic Risk Identification of Steel Buildings with Viscous Dampers*, PhD dissertation, Tokyo Institute of Technology, Tokyo, Japan.

Miyamoto, H. K., and Singh, J. P., 2002. Performance of structures with passive energy dissipators, *Earthquake Spectra* **18**, 105–119.

Miyamoto, H. K., and Gilani, A. S. J., 2008. Design of a new steel-framed building using ASCE 7 damper provisions, *Proceedings of ASCE Structures Congress*, Vancouver, BC, Canada.

Miyamoto, H. K., Gilani, A. S. J., Wada, A., and Ariyaratana, C., 2010a. Collapse risk of tall steel moment frame buildings with viscous dampers subjected to large earthquakes, *The Structural Design of Tall and Special Buildings* **19**, 421–438.

Miyamoto, H. K., Gilani, A. S. J., Wada, A., and Ariyaratana, C., 2010b. Limit states and failure mechanisms of viscous dampers and the implications for large earthquakes, *Earthquake Engineering & Structural Dynamics* **39**, 1279–1297.

National Earthquake Hazards Reduction Program (NEHRP), 2009. *FEMA P695: Recommended Methodology for Quantification of Building System Performance and Response Parameters*, Applied Technology Council, Redwood City, CA.

Pacific Earthquake Engineering Research (PEER) Center, 2009a. *Next Generation Attenuation of Ground Motions (NGA) Project*, University of California, Berkeley.

Pacific Earthquake Engineering Research (PEER) Center, 2009b. *Open System for Earthquake Engineering Simulation (OpenSees)*, University of California, Berkeley.

Taylor Devices, 2009. Personal communication.

Vamvatsikos, D., and Cornell, C. A., 2005. *Seismic Performance, Capacity and Reliability of Structures as Seen Through Incremental Dynamic Analysis, Report No. TR-151*, John A. Blume Earthquake Engineering Center, Stanford University, Palo Alto, CA.

(Received 1 November 2009; accepted 10 January 2011)